Spall formation in solution mined storage caverns based on a creep and fracture analysis

Darrell E. Munson
Sandia National Laboratories*, Albuquerque, NM 87185

REPRINT: Published in the Proceedings of the Fourth North American Rock Mechanics Symposium, Editors J. Girard, M. Liebman, C. Breeds, and T. Doe, A.A. Balkema, Rotterdam, Netherlands, pp. 901-908. 2000.

ABSTRACT: Because of limited direct observation, understanding of the interior conditions of the massive storage caverns constructed in Gulf Coast salt domes is realizable only through predictions of salt response. Determination of the potential for formation of salt spalls, leading to eventual salt falls, is based on salt creep and fracture using the Multimechanism-Deformation Coupled Fracture (MCDF) model. This is a continuum model for creep, coupled to continuum damage evolution. The model has been successfully tested against underground results of damage around several test rooms at the Waste Isolation Pilot Plant (WIPP). Model simulations, here, evaluate observations made in the Strategic Petroleum Reserve (SPR) storage caverns, namely, the accumulation of material on cavern floors and evidence of salt falls. A simulation of a smooth cavern wall indicates damage is maximum at the surface but diminishes monotonically into the salt, which suggests the source of salt accumulation is surface sluffing. If a protuberance occurs on the wall, fracture damage can form beneath the protuberance, which will eventually cause fracture, and lead to a salt fall.

1 INTRODUCTION

The ability to predict fracture of solids has always been a challenging problem. Numerous constitutive models have been proposed in this area, more than can be discussed here. Historically, many of these models have been based on the calculated stresses, and whether or not the stresses exceed a given level, and if so by how much. Typically, these stress based or plasticity models are time-independent and merely indicate the potential susceptibility of the solid to fracture. While these models have served in many situations, it seems reasonable any advanced model must be based on time-dependent damage or fracture evolution criteria.

In the modeling of salt, both for creep and fracture, models have been proposed by Aubertin et al. (1998) and Cristescu (1993) which contain evolutionary aspects and stress or energy fracture criteria. However, the model we utilize here is the Multimechanism-Deformation Coupled Fracture (MDCF) model, which is a micromechanism based continuum damage, evolutionary framework (Chan et al. 1998, 1999). Specifically, the model is used to increase our understanding of the interior behavior of large storage caverns of the Strategic Petroleum Reserve (SPR). Some 62 of these large SPR caverns (roughly 610 m high by 61 m in diameter) are under about 610 m of overburden in the salt domes of the Gulf Coast. Approximately 1220 m long hanging strings of casing are used for transfer of fluids from the caverns. Damage and loss of these hanging strings may be caused by impacts of salt falls from the walls of the cavern, which must involve the failure behavior of salt. However, it is difficult to know cavern conditions and exactly how such salt falls can be produced.

In this work, background evidence is examined which evaluates available internal observations of the caverns of Bryan Mound, one of the four SPR sites, and subsequent events of casing damage. A description of the MDCF model is then given, together with earlier supporting predictions of underground tests. This is followed by numerical

calculational results to investigate potential interior conditions of the SPR caverns using simulations involving first smooth cavern walls and then simple geometric wall protuberances.

---

* Sandia, a multiprogram laboratory operated by Sandia Corporation, a Lockheed Martin Company, for the US Department of Energy (DOE) under Contract DE-AC04-94AL85000.

2 BACKGROUND

Over the years of operation, damage and loss of hanging string casing has occurred periodically in many, but not all, of the SPR caverns in the Bryan Mound, West Hackberry, Big Hill, and Bayou Choctaw salt domes. Munson et al. (1998) studied the possible factors that could contribute to the events of damage and loss. Among a number of possible factors, domal faults or anomalous zone systems, different or irregular cavern geometries, as well as, operational procedures, were eliminated as primary factors. The primary factor appeared to be the material of the dome and the cavern. This material dependence would potentially allow each of the individual caverns within a dome to exhibit different behavior with respect to salt falls, and hence, the different numbers of hanging string damage events. Although the specific nature of the influence of material was not defined, the influence must be upon the fracture characteristics of the salt, as perhaps could be expected.

These large caverns are difficult to study since only indirect access is possible. However, quantitative aspects of the damage event study are of interest because they can reveal some of the interior conditions of the caverns. Wireline tool logs are routinely made to determine the interface between oil and brine and also “tag” the cavern bottom to measure the total cavern depth. The measurements indicate material continues to accumulate with time in the cavern bottoms. The accumulation is believed to be solid salt material from the walls of the cavern because the SPR cavern operation is quiescent and no significant introduction of raw water occurs to cause additional solutioning to release insoluble impurities. The insoluble material in the cavern sump generated from construction solutioning is assumed to not contribute either through extrusion uplift or compaction subsidence to a change in floor elevation, although as a porous material it would probably compact somewhat. From sonic surveys the cavern bottom dimensions are also known, which permits calculation of the yearly rates of accumulation of material in the cavern bottom, as given in Table 1. Also shown are the equivalent number of casing damage events adjusted to give the number for a full length, single hanging string.

Although these results are not definitive, they do suggest two very interesting possibilities about caverns. First, it is apparent that the amount of material falling to the floor differs significantly depending upon the cavern, even though the caverns all are within the same salt dome. The highest rate of nearly 9000 Mg/year (9000 tonnes/year) of BM 112 is almost beyond credence. From this, the range goes down to a mere 71 Mg/year for BM 102. Second, with such large amounts of salt falling, it is almost certain that most of the salt cannot be in large masses. When one realizes that a 0.71 m^3 (0.3 m by 1.0 m by 1.4 m) block, at about a half a tonne, could be expected to do significant damage to a

Table 1. Salt accumulation and hanging string events at Bryan Mound (Munson et al. 1998).

Cav. No.	Bottom Dia. (m)	No. Yr. Accum. (yrs.)	Depth Rate (m/yr.)	Accum. Mass (Mg/yr.)	No. of Events
BM 112	61.0	11	2.59	8945	5
BM 109	79.2	13	1.10	6402	3
BM 103	51.8	12	1.83	4561	5
BM 106	39.6	13	3.08	4490	6
BM 107	54.9	13	0.91	2557	5
BM 113	54.9	10	0.70	1960	2
BM 114	73.2	9	0.61	1520	0
BM 105	73.2	13	0.15	757	0
BM 111	48.8	12	0.30	649	1
BM 101	61.0	12	0.18	631	1
BM 110	27.4	14	0.73	512	0
BM 108	61.0	11	0.12	420	1
BM 115	45.7	10	0.21	414	0
BM 104	48.8	13	0.06	134	0
BM 102	29.0	12	0.09	71	1
BM 116*	?	10	0.61	??	2

* Sonar record unavailable.

casing, the low number of casing events suggest that not many blocks of this size occur. Indeed, if most of the falling salt material were of a large size, it would be impossible to keep a hanging string in the cavern even if many of the blocks missed the casing. This suggests, in general, that most, but not all, of the falling salt masses must be quite small.

The apparent formation of falling masses of salt, regardless of their sizes, suggests the process must involve fracture. Since direct observation of a cavern interior using current technology seems unlikely, any understanding of the process will depend upon analysis of a more fundamental type. As a result, it is necessary to turn to the simulation of potential internal configurations to seek an explanation of the behavior. A model of creep deformation and fracture developed specifically for salt seems nicely applicable for these simulations. Based on an extensive knowledge of the mechanical behavior of salt, the MDCF constitutive model was developed for the WIPP Program. The relevant aspects of the development of this model will be repeated here; but, more complete detail may be found in Chan et al. (1998, 1999).

3 COUPLED CREEP AND FRACTURE MODEL

Fundamentally, we know from recent work (Chan et al. 1998) that a comprehensive constitutive model of salt behavior must describe time-dependent transient and steady state creep, evolution of continuum damage to produce tertiary creep that results in failure, and healing of damage. The concept of micromechanical mechanisms of deformation and fracture, especially through utilization of the deformation mechanism map (Munson & Dawson 1984) and the fracture mechanism map (Ashby, 1983), produces a scientific foundation for the model development. It is essential to note that fracture mechanisms are entirely distinct from plastic deformation mechanisms, even though fracture and deformation may be coupled and their corresponding strains are additive. In contrast to isochoric (constant volume) plastic deformation, non-isochoric fracture processes are highly pressure sensitive. While fracture also normally depends upon the stress direction, here the damage is taken as isotropic.

The MDCF model was initially developed to treat the creep and fracture of salt to support numerical predictions. Later developments of the model have incorporated nonassociated inelastic fracture flow and then extended the model to treat fracture in salt with small impurity inclusions. Thereafter, a fracture healing process known to occur in rock salt was incorporated into the model. This model was used to predict the life of a salt structure underground (Chan et al. 1995). Recently, salt cleavage fracture, although not a time-dependent process, was incorporated since many underground situations involve cleavage fracture.

All of the constitutive model developments were based on laboratory data from triaxial compression tertiary creep testing, from healing kinetics studies, and from indirect Brazilian tensile creep and cleavage tests. The model was validated against the extensive collection of independent in situ data from the very large scale underground tests of the WIPP Program.

The total strain is a sum of the elastic and inelastic strains and the elastic strains and are always included in the model. With this understanding, however, the primary concern is with the inelastic strain. Turning now to just the inelastic strain, the expression for the inelastic strain rate can be represented as a sum of partial differential equations (Chan et al. 1998), as follows:

$$\dot{\varepsilon}_{ij}^{I} = \frac{\partial \sigma_{eq}^{c}}{\partial \sigma_{ij}} \dot{\varepsilon}_{eq}^{c} + \frac{\partial \sigma_{eq}^{\omega_s}}{\partial \sigma_{ij}} \dot{\varepsilon}_{eq}^{\omega_s} + \frac{\partial \sigma_{eq}^{\omega_t}}{\partial \sigma_{ij}} \dot{\varepsilon}_{eq}^{\omega_t} + \frac{\partial \sigma_{eq}^{\omega_h}}{\partial \sigma_{ij}} \dot{\varepsilon}_{eq}^{\omega_h} \quad (1)$$

This generalized, coupled inelastic flow equation is stated in terms of the power-conjugate equivalent stress measures, σ_{eq}^{i}, and equivalent strain measures, ε_{eq}^{i}. Here, as the terms indicate, the indices denote the processes for creep (c), shear damage (ω_s), tensile damage (ω_t), and (h) damage healing, respectively. The superimposed dot is the differential with respect to time. Each of the processes on the right hand side of the equation contain a conjugate stress measure (flow potential) and a conjugate strain rate measure (kinetic equation) for the individual contributions to the flow, as formulated separately in the following sections. However, cavern stress conditions always favor fracture so the term for healing of damage need not be included in the analysis. The complete

constitutive description for creep, fracture, and healing is given by Chan et al. (1998, 1999).

3.1 Creep formulation

Munson et al. (1989) have summarized the initial development of the Multimechanism Deformation (M-D) creep model. It is this model that later formed the basis of the MDCF model. The kinetic creep equation, or strain rate measure, actually results from three dislocation mechanisms identified from the dislocation mechanism map as relevant to the stress and temperature conditions for caverns. These creep mechanisms are all thermally activated and act in parallel. Consequently, the steady state rate is given as the sum of the individual mechanism rates, as follows:

$$\dot{\varepsilon}_S = \sum_{i=1}^{3} \dot{\varepsilon}_{S_i} \tag{2}$$

where the subscripts here denote the i^{th} mechanism. The three micromechanical mechanisms relevant to dislocation controlled processes are (1) dislocation climb controlled creep, (2) an empirically well defined, but unknown mechanism, and (3) dislocation glide controlled creep, respectively, and the individual steady state creep rates for these three mechanisms are given by

$$\begin{aligned}
\dot{\varepsilon}_{S_1} &= A_1 e^{\frac{-Q_1}{RT}} \left(\frac{\sigma_{eq}}{\mu(1-\omega)} \right)^{n_1} \\
\dot{\varepsilon}_{S_2} &= A_2 e^{\frac{-Q_2}{RT}} \left(\frac{\sigma_{eq}}{\mu(1-\omega)} \right)^{n_2} \\
\dot{\varepsilon}_{S_3} &= \left| H\left(\frac{\sigma_{eq}}{1-\omega} - \sigma_0 \right) \right| \left(\sum_{i=1}^{2} B_i e^{\frac{-Q_i}{RT}} \right) \sinh\left[\frac{q\left(\frac{\sigma_{eq}}{1-\omega} - \sigma_0 \right)}{\mu} \right]
\end{aligned} \tag{3}$$

where the A's and B's are structure factor constants, Q's are activation energies, T is the absolute temperature, R the universal gas constant, μ the shear modulus, n's are the stress exponents, q is the stress constant, H is a Heaviside function with the argument $(\sigma_{eq}/(1-\omega)- \sigma_0)$, and σ_0 is the stress limit of the dislocation glide mechanism. The parameter, ω, is a scalar measure of isotropic damage.

The total creep rate is obtained through a transient creep multiplier, F, that acts on the steady state rate of Eq. 2 as given by the function

$$\dot{\varepsilon}_{eq} = F\, \dot{\varepsilon}_s \tag{4}$$

In terms of dislocation concepts the transient response reflects changes in internal defect structure. The defect density increases in workhardening, decreases in recovery, and remains constant in steady state creep. The potentials from the internal defect concentrations drive the transient creep process. As a result, the transient function, F, contains three branches, consisting of a workhardening branch, a steady state branch, and a recovery branch, respectively, as follows:

$$F = \begin{cases} e^{\Delta\left(1-\frac{\zeta}{\varepsilon_t^*}\right)^2} & ;\ \zeta < \varepsilon_t^* \\ 1 & ;\ \zeta = \varepsilon_t^* \\ e^{-\delta\left(1-\frac{\zeta}{\varepsilon_t^*}\right)^2} & ;\ \zeta > \varepsilon_t^* \end{cases} \tag{5}$$

Here, Δ and δ are the workhardening and recovery parameters. The isotropic transient strain state parameter, ζ, is an internal state parameter that traces the transient strain evolution. Workhardening and recovery parameters are functions of the stress, as follows:

$$\begin{aligned}
\Delta &= \alpha_w + \beta_w \log\left(\frac{\sigma_{eq}}{\mu(1-\omega)} \right) \\
\delta &= \alpha_r + \beta_r \log\left(\frac{\sigma_{eq}}{\mu(1-\omega)} \right)
\end{aligned} \tag{6}$$

where the α's and β's are constants; however, under most typical cavern loading situations, δ, itself, may

be approximated as a constant. The transient strain limit, ε^*_t, is given by

$$\varepsilon_t^* = K_0 e^{cT} \left(\frac{\sigma_{eq}}{\mu(1-\omega)} \right)^m \tag{7}$$

where K_0, c, and m are constants. The evolutionary rate of the isotropic transient strain state parameter is governed by

$$\dot{\zeta} = (F-1)\dot{\varepsilon}_s \tag{8}$$

As is apparent, the evolutionary rate of the transient strain state parameter must become zero during steady state creep.

The conjugate equivalent stress measure or flow potential to be used in Eq.1 that applies to the creep process is

$$\sigma_{eq}^c = |\sigma_1 - \sigma_3| \tag{9}$$

which is twice the Tresca maximum shear stress. This measure has been shown experimentally from multiaxial, hollow cylinder tests on salt to be preferred over other measures (Munson et al. 1989). Furthermore, the close agreement between numerical simulations of underground room closures and the data obtained at the Waste Isolation Pilot Plant (WIPP) facility tend to confirm this model, as well as this flow potential.

These equations differ from those originally developed for the M-D model by the inclusion of the damage parameter. The damage has the effect of decreasing the area over which the force is applied, thereby increasing the effective stress (not the applied stress, which remains constant) and hence the creep rate increases.

3.2 Fracture formulation

The kinetic, conjugate strain rate equations for shear and tensile damage-induced inelastic flow are developed from the concept of microfractures that undergo shear deformation to produce wing-tip cracks. The crack deformation then results in both shear and dilational strains. It is thought the cracks occur at the ends of dislocation slip bands and, as a result, the form of the kinetic equation is taken of the same form as that previously developed for dislocation glide. Thus, from Chan et al. (1998)

$$\dot{\varepsilon}_{eq}^{\omega i} = F^{\omega i} \dot{\varepsilon}_s^{\omega i} \tag{10}$$

where "*i*" indicates either the shear or the tensile damage component and $F^{\omega i}$ is a transient function for the respective mode of damage. The transient function for damage is given by

$$F^{\omega i} = F \ \exp\left[\frac{c_4 (\sigma_{eq}^{\omega i} - c_5)}{\chi_7} \right] \tag{11}$$

where c_4, c_5, and χ_7 are constants. Fracture and creep are clearly coupled because F is the transient function from the creep deformation formulation. Then, the kinetic equations for damage induced flow during steady state creep are expressed as

$$\dot{\varepsilon}_s^{\omega i} = c_1 \omega_0 e^{c_3 \omega} \left[\sinh \left(\frac{c_2 \sigma_{eq}^{\omega i} H\left(\sigma_{eq}^{\omega i}\right)}{\mu (1-\omega)} \right) \right]^{n3} \tag{12}$$

$$c_1 = c_0 \left(\sum_{k=1}^{2} B_k e^{\frac{-Q_k}{RT}} \right)$$

where c_0, c_2, c_3, and n3 are constants, and ω_0 is the initial value of the damage variable, ω. The structure factors are summed over the *k* indices on B and Q.

The damage evolution equation is of the form

$$\dot{\omega} = \chi_0 \left\{ \left[\frac{\sigma_{eq}^{\omega_s} H\left(\sigma_{eq}^{\omega_s}\right)}{\chi_s} \right]^{\chi_{3s}} + \left[\frac{\sigma_{eq}^{\omega_t} H\left(\sigma_{eq}^{\omega_t}\right)}{\chi_t} \right]^{\chi_{3t}} \right\} \tag{13}$$

$$\chi_0 = \frac{\chi_4}{t_0} \omega \left[\ln\left(\frac{1}{\omega}\right) \right]^{\frac{\chi_4 + 1}{\chi_4}}$$

where χ_4, χ_s, χ_t, χ_{3s}, and χ_{3t} are constants; t_0 is a reference time.

As initially noted, damage in compression is considered to arise from shear sliding of microcracks and by dilatant opening of the wing-tip cleavage cracks that can develop on the shear cracks. The

resulting inelastic flow includes deviatoric and dilational components. Normally, each of these components would require just one individual stress measure for use in Eq.1, for a total of two (2) stress measures. However, in fact, we will have to define three (3) stress measures for the fracture flow. Unlike the creep deformation, the shear component of the fracture strain is nonassociated and therefore requires the use of two (2) conjugate stress measures in Eq. 1. This was found necessary to adequately represent the experimental data, a situation that is not uncommon. To differentiate between these two measures, the shear flow stress measure will have a subscript *f*, while the shear kinetic equation stress measure will have a subscript *k*. Thus, the conjugate stress measure or flow potential of Eq.1 for the shear component of fracture is

$$\sigma_{eq}^{\omega} \Big|_f^s = \left|\sigma_1 - \sigma_3\right| - \frac{\chi_2 \chi_8}{3}\left[I_1 - \sigma_1\right] \quad (14)$$

and the comparable nonassociated, conjugate stress measure for use in the kinetic equation, Eq. 1, for the shear component of fracture is

$$\sigma_{eq}^{\omega_s} = \left|\sigma_1 - \sigma_3\right| - f_p \chi_2 \chi_7 \operatorname{sgn}\left(I_1 - \sigma_1\right)\left[\frac{I_1 - \sigma_1}{3\chi_7 \operatorname{sgn}\left(I_1 - \sigma_1\right)}\right]^{\chi_6} \quad (15)$$

and the conjugate stress measure for use in the flow law and the kinetic equation for the tensile component is given by the following:

$$\sigma_{eq}^{\omega} \Big|_f^t = -\chi_1 \sigma_3 H\left(-\sigma_3\right) \quad (16)$$

here, χ_1, χ_2, χ_6, χ_7, and χ_8 are constants and f_p is a parameter related to volume and effectiveness of the impurity content to promote fracture.

The pressure dependence of fracture is contained in Eq. 15, where the second term on the right hand side of the equation is essentially a pressure term that diminishes the magnitude of the equivalent conjugate stress as pressure increases. The shear stress ($J_2^{1/2}$)-pressure (I_1) invariant relationship is shown in Figure 1 for clean salt. The curve shown is the boundary along which the damage rate is zero. Damage evolves for all stress states above and to the left of the curve; while damage is suppressed for all stress states below and to the right of the curve. Healing of previously damaged salt can take place only for stress states within the region below and to the right of the curve, which is the region of damage suppression.

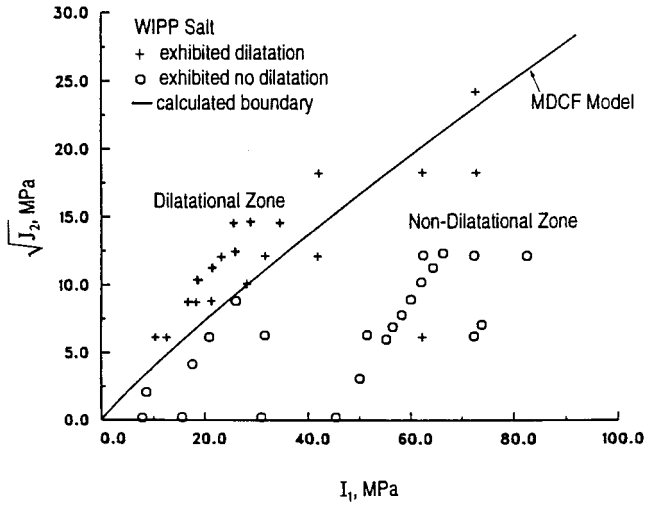

Figure 1. Damage boundary between dilatant and non-dilatant creep behavior (Chan et al. 1998).

Impurities that form particles in salt can have a rather significant effect on the fracture behavior. Particles alter the local stress field to decrease the effective confining pressure, which in turn, through the pressure term of Eq. 15, permits microfractures to form more readily (Chan et al. 1998), according to

$$f_p \cong 1 - p_1 \rho \quad (17)$$

where p_1 is a constant and ρ is the volume fraction of impurity particles. Other second phase (anhydrites, polyhalites) impurities, not in the form of particles, would probably not have the same effect. The effect of particles on the zero damage curve of Figure 1 is to displace the curve to lower shear stress ($J_2^{1/2}$) values as the particle content increases.

4 PREVIOUS APPLICATIONS

The MDCF model permits calculation of the life expectancy of a room (Chan et al. 1995) by taking the practical limit of damage at failure to be about 0.15. At this level of damage, laboratory observations indicate the salt no longer has integrity.

There are a series of four test rooms at the WIPP that were excavated early in the project. The rooms are at the storage horizon of 655 m and have dimensions of 3.96 m height by 10.06 m width and 91.44 m length. Rooms were separated by 30.48 m thick pillars. Physical observations (Borns & Stormont 1989) documented the massive failures. Observable fracture in the rooms occurred in the floor and roof, with indirect indications of slabbing fractures in the ribs. The loss of rib integrity was suggested by unconstrained flow through the subparallel fractures from pressurized boreholes. Floor fractures caused scallop shaped fractures. These fractures began with thin edges near the rib-floor junction and continued downward to penetrate into the floor until they intersected a massive anhydrite layer about 1.0 m beneath the floor, at about quarter room span. Floor fractures were verified by visual surface observations and by large diameter core holes drilled into the floor. After 8 and 11 years, the unsupported roofs of two rooms fell to reveal massive inverted, shallow bowl shaped slabs, thin at the edges near the intersection of the room ribs and roof and thick at the middle in the room center.

The damage around a room was calculated using an approximation of an infinite series of rooms with symmetry planes at mid-room span and mid-pillar thickness (Chan et al. 1995). Results at 10 years of the MDCF calculation through a room cross-section are shown in Figure 2. The concentration of damage occurs in the floor in the scallop configuration consistent with the observed fractures. Ribs and roof also show the damage consistent with the formation of the observed slabs. Roof damage at 10 years is consistent with the observed failure times. Two unsupported room roofs fell at 8 and 11 years.

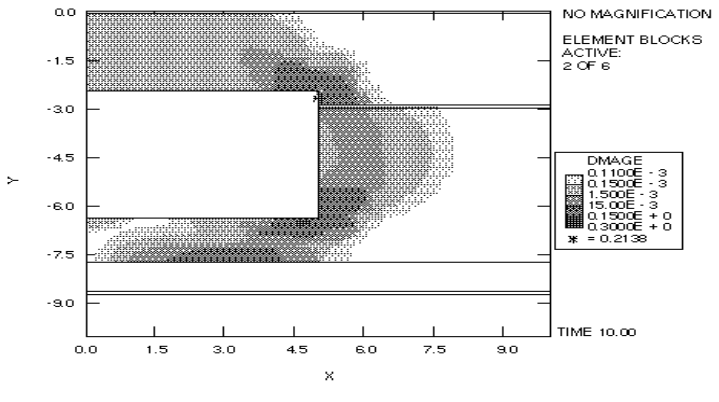

Figure 2. Damage around underground room (Chan et al. 1995).

5 SIMULATION OF CAVERN CONDITIONS

The simplest simulation is of just a smooth walled cavern. In this case, the calculational mesh is a "pineapple slice" with the stress appropriate to the depth applied to the top and bottom of the slice and the internal cavern pressure applied inside the "hole." This is permits an axisymmetric calculation modeling the radial creep and damage behavior of a cylindrical shaft or cavern. For the SPR caverns, the differential stress (or driving stress) for creep is the difference between the overburden (lithostatic) and the internal fluid pressures. The overburden consists of near-surface earth, cap rock, and salt, in that order with depth. The caverns store crude oil, normally under slightly pressurized conditions. The lithostatic stress of course depends upon depth and the fluid pressures will vary with fluid type (gas for instance) and operation practice. For caverns of the typical SPR configuration, the pressure differential between the cavern interior and the surrounding salt at the maximum cavern depth, where maximum damage would also be expected, is approximately 14.7 Mpa. Calculational results using SPECTROM-32, were initially made for WIPP for the equivalent situation (Munson et al. 1999), as shown in Figure 3. The damage increases with time, but decreases with distance (nondimensionalized to multiples of cavern radii), into the salt. In the calculation, the impurity content was assumed to be about 3.0%, equivalent to the WIPP argillaceous halite.

Interestingly, the calculated damage is quite small, even though all the conditions of material and stress were selected to produce the maximum damage possible. At the top of the cavern, no damage is calculated. Moreover, if clean salt properties were used in the calculation rather than the 3.0% impurity salt properties, virtually no damage would be calculated anywhere. As the results suggest, the caverns are resistant to the development of damage, and hence fracture, because

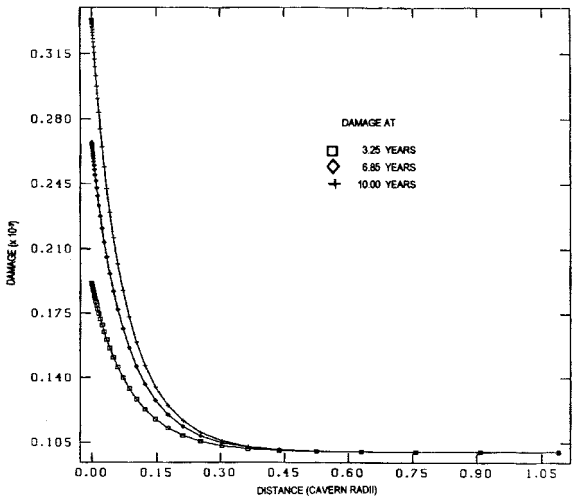

Figure 3. Radial damage distribution into a cavern wall (Munson et al. 1999).

of their favorable configuration. Stresses around the cavern are largely compressive. Creep closure occurs of course, but the stress condition around the cavern is one that largely suppresses damage formation. Under these conditions of a smooth walled, cylindrical cavern, the results suggest the maximum damage always is at the cavern wall. Fracture, if it occurs, probably results only in the gradual loss of material from the wall surfaces. It is possible that much of the observed accumulation of material on the cavern floor with time may be produced in this manner.

As a result, to produce the more massive blocks of material of a salt fall requires a somewhat different scenario. Two calculations were made based on protuberances of the cavern wall, one a protruding bump with a semicircular cross-section forming a ring around the interior of the cavern wall, and the other a semicircular bump running vertically down the wall of the cavern. The results for the first protuberance was uninteresting in that all portions of the wall and protuberance moved inward uniformly by creep. Strain concentrations did not occur and the damage field would be as in Figure 3. However, this was not true of the second geometric protuberance. The mesh for the two dimensional SANCHO M-D calculation of the second protuberance, as seen looking down the cavern axis, is shown in Figure 4. In this situation, the radial strain distribution through the bump has a maximum at the root (about 0.45 of the protuberance radius) of the bump, as shown in Figure 5, and not at the surface of the bump. While the M-D model does not give damage, an uncoupled

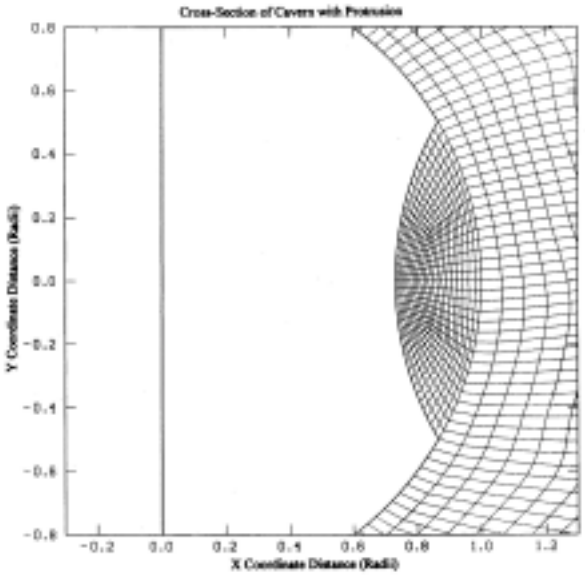

Figure 4. Calculational mesh for vertical wall protuberance.

calculation shows a sharp damage peak ($\omega = 0.0021 \times 10^{-3}$) between the depth rations of 0.15 and 0.45 (with the peak at about the root depth of 0.30). This suggests the salt will fail and separate at the root of the bump, precisely the conditions for development of a spall prior to a salt fall.

The latter of these calculations suggest certain protuberances can act as preferred sites for generation of salt spalls. Sonar surveys do illustrate that cavern walls can be irregular. Moreover, the material impurities, as well as the geometric details, must be important factors in the process.

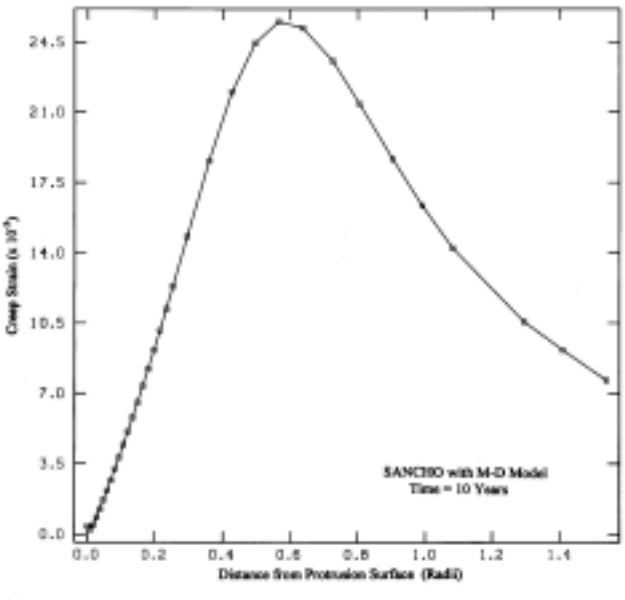

Figure 5. Radial creep strain at protuberance center against protuberance radii.

6 SUMMARY

The MDCF model and analysis system was used to simulate the expected behavior of a cylindrical cavern in salt. While damage is generated uniformally around the cavern wall, it is not as pronounced as might be expected. Damage is a function of the depth in the cavern, and is maximum at the bottom of the cavern. However, this uniform damage probably explains the sluffing of material that accumulates on the cavern floor. In further simulations, a very simple axial cylindrical protuberance geometry was shown to have a localized damage zone at the root of the protuberance which suggests that continued damage would lead to failure and spall of the protuberance. These kinds of geometric situations could explain the creation of salt falls. Both the sluffing and spall are influenced by the impurity content of the salt, but spall creation must also be sensitive to the geometric configuration.

REFERENCES

Ashby, M.F., 1983. Mechanisms of deformation and fracture, *Advances in Applied Mechanics*, **23**, 117-177.

Aubertin, M., J. Sgaoula, S. Servant, M.R. Julien, D.E. Gill & B. Landanyi, 1998. An up-to-date version of SUVIC-D for modeling the behavior of salt, *Proc. 4th Conf. on the Mech. Behavior of Salt*, Trans Tech Pub., Clausthal-Zellerfeld, Germany, 205-220.

Borns, D.J., & J.C. Stormont, 1989. The delineation of the disturbed rock zone surrounding excavations in salt, *Proc. 30th U.S. Symp. on Rock Mech.*, A.A. Balkema, Rotterdam, Netherlands, 353-360.

Chan, K.S., K.L. DeVries, S.R. Bodner, A.F. Fossum & D.E. Munson, 1995. A damage mechanics approach to life prediction for a salt structure, *Computational Mechanics '95*, Vol. 1, 1140-1145.

Chan, K.S., D.E. Munson, A.F. Fossum & S.R. Bodner, 1998. A constitutive model for representing coupled creep, fracture, and healing in rock salt, *Proc. 4th Conf. on the Mech. Behavior of Salt, Trans Tech Pub.*, Clausthal-Zellerfeld, Germany, 221-234.

Chan, K.S., D.E. Munson & S.R. Bodner, 1999. Creep deformation and fracture in rock salt, Ch. 11, *Advances in Fracture Mechanics*, ed. M.H. Aliabadi, WIT Press, Boston, pp. 331-379.

Cristescu, N., 1993. A general constitutive equation for transient and stationary creep of rock salt, *Int'l J. Rock Mech. Min. Sci. & Geomech. Abstr.*, **30**, 125-140.

Munson, D.E. & P.R. Dawson, 1984. Salt constitutive modeling using mechanism maps, *Proc. 1st Conf. on the Mech. Behavior of Salt*, Trans Tech Pub. Clausthal-Zellerfeld, Germany, 717-737.

Munson, D.E., A.F. Fossum & P.E. Senseny, 1989. *Advances in Resolution of Discrepancies between Predicted and Measured In-Situ WIPP Room Closures*, SAND88-2948, Sandia National Laboratories, Albuquerque, NM.

Munson, D.E., M.A. Molecke & R.E. Myers, 1998. Interior cavern conditions and salt fall potential, *Proc. Solution Mining Research Institute Spring Meeting 1998*, El Paso, TX, SMRI, Deerfield, IL, 226-239.

Munson, D.E., A.F. Fossum & K.S. Chan, 1999. Fracture and healing of rock salt related to salt caverns, *Proc. Solution Mining Research Institute Spring Meeting 1999*, Las Vegas, NV, SMRI, Encinitas, CA, 67-89.